ARCHIVE OF MECHANICAL ENGINEERING

DOI: 10.24425/ame.2022.140417 2022, Vol. 69, No. 2, pp. 269–300

Kuldeep KUMAR [1], Rajesh Kumar VERMA [1]

Measurement and evaluation of delamination factors and thrust force generation during drilling of multiwall carbon nanotube (MWCNT) modified polymer laminates

Received 7 August 2021, **Revised** 19 January 2022, **Accepted** 8 February 2022, **Published online** 26 April 2022

Keywords: drilling, glass fiber, MWCNT, delamination, thrust

In recent years, manufacturing industries have demanded high-performance materials for structural components development due to their reduced weight, improved strength, corrosion, and moisture resistance. The outstanding performance of polymer nano-composites substitutes the use of conventional composites materials. This study is concerned with the machining of MWCNT and glass fiber-modified epoxy composites prepared by a cost-effective hand layup procedure. The investigations were carried out to estimate the generation of the thrust force (Th) and delamination factors at entry (DF_{entry}) and exit (DF_{exit}) side during the drilling of fiber composites. The effect of varying constraints on the machining indices was explored for obtaining an adequate quality of hole created in the epoxy nano-composites. The outcome shows that the feed rate (F) is the most critical factor influencing delamination at both entry and exit side, and the second one is the thrust force followed by wt.% of MWCNT. The statistical study shows that optimal combination of S (1650 Level-2), F (165 Level-2), and 2 wt.% of MWCNT (Level-2) can be used to minimize DF_{entry}, DF_{exit}, and Th. The drilling-induced damages were studied by means of a high-resolution microscopy test. The results reveal that the supplement of MWCNT substantially increases the machining efficiency of the developed nano-composites.

1. Introduction

Fiber-reinforced polymer (FRP) composites extensively replace conventional manufacturing materials such as metals and alloys in the manufacturing sector. Due to unique structural properties, it is highly preferred to apply them in trans-

✉ Rajesh Kumar VERMA, e-mail: rkvme@mmmut.ac.in

[1] Materials and Morphology Laboratory, Department of Mechanical Engineering, Madan Mohan Malaviya University of Technology, Gorakhpur, India; ORCIDs: K.K.: 0000-0002-3131-9247; R.K.V.: 0000-0002-3973-4779

portation, aerospace, sporting goods, components, etc [1–3]. In particular, the glass fiber-reinforced polymers (GFRPs) are typically used in aircraft and sports products like golf shafts, bicycle helmets, etc [4–6]. But, the fragile nature of glass fiber restricts some specific functions subjected to fatigue and creep conditions. To overcome this limitation, the addition of some other secondary reinforcement is used to strengthen the properties of GFRP composites. Nano-dispersed fillers are preferable over micro-fillers in this case because of their higher aspect ratio, higher surface area, reduced angularity, and lower volume required [7]. The aerospace and automotive sectors are trying to minimize weight of their products by around 50 percent by replacing primary structural components with ones fabricated from polymer composites [8, 9]. In this sector, fuel consumption and passenger comforts are improving owing to lightweight glass/polymer composites. The nanofillers contribute to the effective transfer of load from the matrix to the reinforced particles of the strong interface. Carbon-based nanofillers (CBNs) improved the fracture toughness of polymer matrix without wortening their thermomechanical properties [10, 11]. The use of graphene, carbon nanotubes (CNTs), carbon nanosheets (CNS), and other CBNs improves composite properties. These nanomaterials have been extensively explored since the discovery of carbon allotropic forms [12]. The carbon nanofiller is a valuable additive for modifying epoxy structure properties. CNTs are extremely desirable nanoparticle reinforcements for epoxy matrix and metal composites [13, 14]. The multi-walled carbon nanotubes (MWCNTs) are extensively used in high precision component manufacturing due to excellent features, such as high aspect ratio, strong electric conductivity, and high fracture strain [15, 16]. Tabatabaeian and Ghasemi [17] examined the effect of nanomaterials on the structural performance of polymer composite. The GFRP composites were modified by adding MWCNT (0% and 1%) as supplement materials. The addition of 1% of MWCNTs reduced residual stress and delamination effect by 30% and 2.33%, respectively. The findings showed a considerable improvement of the mechanical strength and thermal properties of the developed nano-composite. Gaurav and Singh [18] developed laminate composites to assess the fatigue life and tensile test. The MWCNT supplement expanded the absorptivity of the solution in the Ultraviolet-Visible Region (UV–Vis), reflecting a larger number of disentangled and separate MWCNTs in the solution. Shivamurthy et al. [19] examined the structural property of the MWCNT/Glass fiber modified epoxy nano-composite. It was shown that the MWCNT increased the mechanical quality and reduced wear of the proposed composite. The researchers concluded that the composite with 0.3 wt % of MWCNT exhibited better properties than those with 0.07% and 0.15 wt % of MWCNT.

The composite material undergoes various machining processes like milling, drilling, turning, etc., to assemble different components for specific applications [20]. Drilling is an effective machining procedure in polymer manufacturing for its high efficiency in constructing mechanical joints and product assem-

bly [21, 22]. However, the findings demonstrate that GFRP is prone to production flaws such as burr formation, shearing, delamination, and thermal degradation. It is mainly due to its fragile, non-homogeneity, and anisotropic behavior. Delamination is one of the most common flaws in drilled components, reducing mechanical strength and fatigue life [23]. In the processes of drilling of the polymer composite, thrust, torque, tool wear, delamination, and surface quality can be controlled by varying machining factors like feed rate, speed, and tool characteristics [24, 25]. Manufacturing requires the best machining performance, i.e., the finest quality hole with a minimal amount of damage and a perfectly machined surface. It can be achieved by controlling machining parameters using optimization modules for efficient machining of the product with reduced machining defects. Several well-known researchers have proposed efficient optimization modules and theories to control the process parameters during composite machining. The primary drilling parameters like drill speed, feed rate and tool geometry were investigated for improving machining performance. In this domain, Poor et al. [26] investigated drilling operation on carbon/polymer composite and discussed the burr formation mechanism and burr measurement technique. Their findings reveal that the depth of cut, cutting edge radius angle, and fiber cutting angle are the most important parameters in drilling polymer composite. Higuchi et al. [27] studied push-out delamination at the exit side in drilling of a polymer composite. For evaluating the push-out delamination, they used X-ray computer tomography and optical microscopy. Kumar et al. [28] examined the drilling performance of CFRP/epoxy nano-composites modified by graphene oxide (GO). For the drilling test, three process constraints, namely, cutting speed, feed, and wt.% of GO were varied at three levels. The overall objective of this work was to obtain the desired values of surface roughness, thrust force, torque, delamination on entry and exit side by controling the process parameters. The optimal parametric setting was estimated by a hybrid module of combined quality loss (CQL) and WPCA. The correlation factor between the machining responses was evaluated by the principal component analysis (PCA) tool. Finally, the authors stated that the cutting velocity is the most dominant factor, followed by the feed rate and wt.%. Hoffmann et al. [29] investigated the hole quality and delamination factor of air-cooled drilled polymer composite. They used an uncoated carbide drill toll, and applied varying feed rate and cutting speed for drilling of CFRP composite. They stated that minimum damage and low delamination factor were observed at a high cutting speed. The researchers concluded that the compressed cooling reduced the delamination at the entry side of the hole. The delamination at the exit side increased when the push-down effect increased compared to the dry cutting. Erturk et al. [30] studied the effect of cutting temperature and conducted a parametric optimization in drilling a continuous GFRP composite. The drilling operation was performed under dry conditions, and there were chosen three three-level factors, such as drill bit (HSS-R; HSS-TiN; carbide), spindle speed (535;

1720; 3030), and feed rate (01; 02; 03). The outcomes showed that material temperature slightly increased as the spindle speed increased. The highest temperature was produced during the drilling operation with the HSS-R drill bite compared to the HSS-TiN and carbide drill bit. They also concluded that the thrust force and the torque increase as the feed rate increases. Pramod et al. [31] performed the drilling operation on nano-polymer composite and investigated the delamination induced in the drilled holes. The experimentation was performed by means of the Taguchi L16 orthogonal array. The authors reported that minimum delamination was observed in drilling the nano-composite (nano clay and graphene) compared to the base composite. The minimum delamination and circularity error were observed at a higher spindle speed, lower feed rate, and a smaller drill bit. Kharwar et al. [32] performed the milling test on the MWCNT/epoxy nano-composite samples. The authors investigated the milling behavior and determined an optimal parametric set using an algorithm based on the Particle Swarm Optimization (PSO) approach. The milling efficiency was explored by variation of four factors at three different levels during the machining test. For this, MWCNT wt.%, the spindle speed, the feed rate, and the depth of cut were considered to acquire the desired surface roughness and material removal rate (MRR) values. It was observed that the MRR reduces at higher loading of MWCNT wt.%, and a smooth surface can be obtained at a higher spindle speed. The surface roughness rises with an increase in the feed rate due to the strain hardening effect. Gokulkumar et al. [33] varied the drilling factors such as speed and feed rate to achieve the optimum thrust force value during drilling of GFRP composites. It was observed that higher thrust forces could be obtained at lower cutting speeds. Liu et al. [34] used aramid fibers to fabricate polymer composites applicable for various functions in the aircraft and automotive components. The aramid modified composites were drilled to examine the delamination failure. The number of uncut fibers determined the delamination by the chisel edge during drilling. Bhushi et al. [35] elaborated algorithms and metaheuristics tools, like Particle Swarm Optimization (PSO), Simulating annealing (SA) and Genetic Algorithm (GA) to examine the delamination generation in the drilling of carbon fiber reinforced laminate composites. The response surface-based regression equation was derived for modeling and simulation of varying parameters. ANOVA results showed that feed rate and tool helix angle were the most significant factors for drilling efficiency. PSO algorithm findings for delamination values were remarked as more feasible than GA and SA for optimization purposes. Janakiraman et al. [36] examined the cryogenic condition for the drilling test. The response was examined by regression modeling of delamination factors, surface roughness, and the thrust force. Mudhukrishnan et al. [37] used a 6 mm diameter HSS, tipped, and solid carbide tool for the drilling processes. The thrust force directly increased with the feed rate. The authors observed that the HSS tool produced a greater thrust variation compared to tipped carbide and solid carbide tools. Kwon et al. [38] studied delamination

and uncut fibers during machining of the CFRP composite. They concluded that a smaller thrust force produces less delamination, but the thrust force creates more delamination damage when increased. Panneerselvam et al. [39] experimented with the machining effect of delamination on the Sisal-GFRP composite. The experiments were designed by the Taguchi method to assess the delamination factors. The researcher applied the signal-to-noise ratio (S/N) to establish operating conditions for obtaining minimal amount of delamination. During the drilling performance, minimum delamination damage occurred at a higher spindle speed. Minimum thrust force and torque were observed at a lower drill feed value.

Several authors investigate the machining aspects of polymer composites reinforced with macro-fibers like glass, carbon, aramid, etc. The studies related to polymer nano-composites are passing through the transition phase. Most of the studies are limited to the synthesis and characterization phase only. Exploring exceptional features of modified nano-composites is not feasible without understanding the machinability efficiency and optimization of the process parameters. During modified composite machining, delamination is observed causing significant damages that may lead to rejection of the entire product assembly. Delamination reduces durability and effectiveness of the machined components. The intermittent cutting force control is another critical challenge for polymer manufacturers. It could be dealt with through the balancing of varying parameters using a simultaneous optimization module. Numerous publications shows the feasibility of the modified nano-composites for high-performance applications in aircraft, aerospace and defense products, etc. Proper cutting condition and damage-free machining are complex tasks due to anisotropy and low ductility of glass fiber/polymer composites. This article explores the fabrication and estimates drilling machinability of MWCNT incorporated GFRP/epoxy nano-composites. It has been remarked that glass fiber is a promising and economical substitute to conventional composites due to its outstanding properties and cost-effectiveness [40–44]. The supplement of MWCNT/Glass fiber could produce the desired structural function properties [45–48]. This work shows the machining aspect of the fabricated nano-composite samples during the drilling test.

The machinability-related studies will provide an insight into selection of optimal process parameters for an efficient machining environment. It is only feasible by a comprehensive experimented analysis and applying statistical models relating response and parameters. The RSM-based Box Behnken design (15 tests) was applied to perform the experimentations. The delamination factors at the entry (DF_{entry}) and exit side (DF_{exit}) of the sample, and the thrust force (Th) in the machining (drilling) of MWCNT incorporated GFRP/epoxy nano-composite were examined. Drilling experiments were carried out in varying cutting conditions, such as speeds, feed rates, and wt.% of MWCNT. Therefore, it was necessary to consider the effect of each process constraint on machining indices through mathematical modeling and optimization tools. The present work identifies the parametric effect

and suggests an efficient way to control the defects and fracture during drilling of the laminated composite. The role of MWCNT is well described in this study for the development of a multi-function composite. An effort has been made to modify the conventional fiber (macro size) composite by substituting it with a high-strength polymer nano-composites.

2. Experimentation

2.1. Development of polymer nano-composites

The material used for the study was the Glass Fiber Reinforced Polymer (200 gsm), acquired from M/s/CF composites Delhi Pvt. Ltd. India, and epoxy-based on bisphenol purchased from by M/s. AE Services, Karnataka, Bangalore, India. The nano-composite was fabricated using caste-effective hand layup process with varying 01, 02, and 03 wt.% of MWCNT and employing an ultra sonicator for nanofiller dispersion, with epoxy resin supplied by M/s. AD-Nano Technology private Ltd. Karnataka India. To strengthen the composite, the Lapox L-12, bisphenol-based epoxy resin and K-6 Hardener were mixed up to a ratio of 10:1 by weight for the preparation of composite laminates. MWCNTs are frequently obtained as agglomerates. To deagglomerate them, high-quality ethanol was added, followed by 1 hour of sonication at 40 kHz using an ultrasonicater machine. The properties of the MWCNT nano-material are listed in Table 1. After sonicating the MWCNT, the solution was thoroughly stirred with a mechanical stirrer at 450 RPM for 1 hour at 85°C to facilitate the dispersion of CNTs into the epoxy matrix. After mechanical stirring, the mixed epoxy and MWCNT solution was keep at room temperature for cooling for about one hour. The hardener was blended in a 10:1 ratio and physically laid up between silicon rubber sheets with overhead projection sheets on both sides after the number of layers was adjusted. The sheets were sprayed with a mold releasing agent to prevent the laminate from sticking to them. During the quaring cycle, the composite was pressed under a load of 5 kN for 24 houres. The developed composite (size of $100 \times 100 \times 5$ mm) is shown in Fig. 1.

Table 1. MWCNT specifications

S. N	Factors	Feature
1	Form	Multiwall Carbon Nanotube
2	Purity	Gretter than 99%
3	Average diameter	10–15 nm
4	Average length	5 μm

X-ray diffraction (XRD) imaging was performed on the prepared nano-composite to confirm nanomaterials' chemical composition and homogenous dispersion.

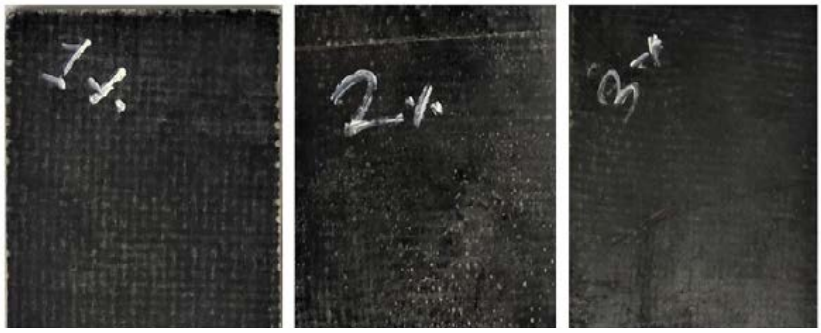

Fig. 1. Prepared sample (1, 2, and 3 wt.% of MWCNT)

The XRD is commonly used to evaluate the degree of graphitization and nanotubes [49–53].

Fig. 2 shows the synchrotron XRD spectrum of pure MWCNT, neat GFRP/epoxy, 0.1 and 0.3 wt.% of MWCNT GFRP composites samples. Pure MWCNT exhibits high peaks at 2θ = 27.10 degrees and lower peaks at 2θ = 38, 20, and 41.1 degrees, indicating the presence of graphitic plane in the sample. The lower peaks at 2θ = 27.10 degrees and higher peaks at 2θ = 79.50 and 38.20 degrees are found in the epoxy nano-composites. It confirms the presence of the graphitic plane in the sample [54, 55]. Table 2 represents mechanical properties of the proposed epoxy nano-composites.

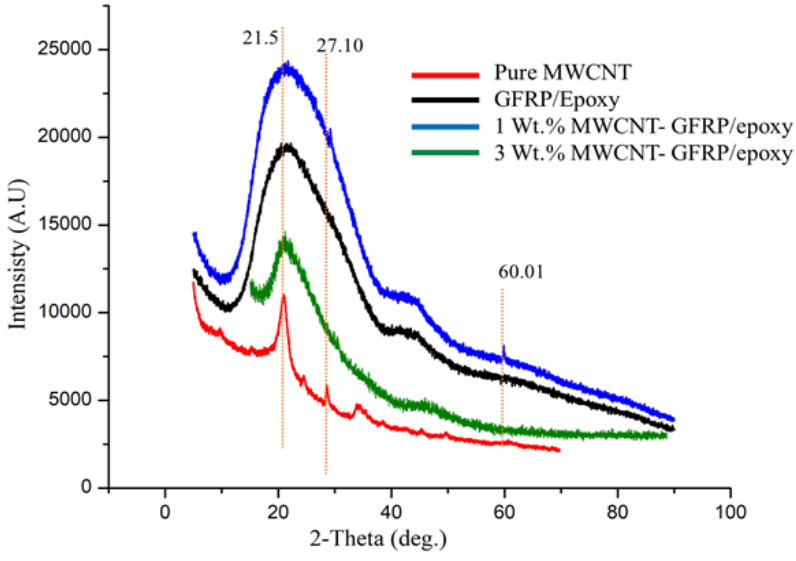

Fig. 2. XRD pattern of pure MWCNT and 1 wt.% MWCNT/GFRP composites

Table 2. Mechanical properties at 1, 2, and 3 wt.% of MWCNT/GFRP samples

Materials		Tensile properties	Flexural properties
Sample code	MWCNT content (wt.%)	Tensile strength (MPa)	Flexural strength (MPa)
1% MWCNT-GFRP	1	158.88	184.83
2% MWCNT-GFRP	2	133.96	151.27
3% MWCNT-GFRP	3	128,32	131.27

3. Design of experiment

3.1. Response surface methodology (RSM)

Box and Draper designed the response surface methodology (RSM) to fit experimental parameters to models. RSM is a set of numerical approaches for constructing mathematical models and estimating factor effects in order to find the best variable resolution. In the model generation stage, RSM employs the statistical design of experiments and the least-square fitting approach [56–59]. This approach aims at obtaining a good relationship between various input drilling parameters and the output response, and optimizing the response prediction.

If a linear function of independent variables properly models the response, the approximation function is the first-order model. The 1st order mathematical model can be explained by the following Eq. (1).

$$y = \beta_0 + \beta_1 x_1 + \beta_2 x_2 + \ldots + \beta_k x_k + \epsilon\,. \tag{1}$$

In general, the 2nd order polynomial response surface model is used to study the influence of machining parameters on the responses. The 2nd order mathematical model can be explained by the following Eq. (2).

$$y = \beta_0 + \sum_{j=1}^{k} \beta_j x_j + \sum_{j=1}^{k} \beta_{ij} x_j^2 + \sum_{i}^{k-1} \sum_{j}^{k} \beta_{ij} x_i x_j + \epsilon, \tag{2}$$

where $i = 1, 2 \ldots, k-1$ and $j = 1, 2, \ldots, k$ also $i < j$.

The RSM design was used to perform fifteen drilling tests for experimentation (Table 3) [60]. The three varying parameters, namely, the spindle speed (S), the feed rate (F), and wt.% of MWCNT were considered at three different levels (Table 3) of CNC vertical milling machine setup (Model-BMV35-TC20). An electric Kistler dynamometer was attached to record the data generated by the thrust force (Th) during the drilling process. TiAIN Sic coated drill bits (5 mm diameter) were used, as described in Fig. 3. The specification of the machining setup is presented in Table 4.

Table 3. Process parameters

Factors	Nomenclature	Level			Unit
		1	2	3	
Spindle speed	S	850	1650	2450	rpm
Feed rate	F	85	165	245	mm/min
wt.%	MWCNT	1	2	3	–

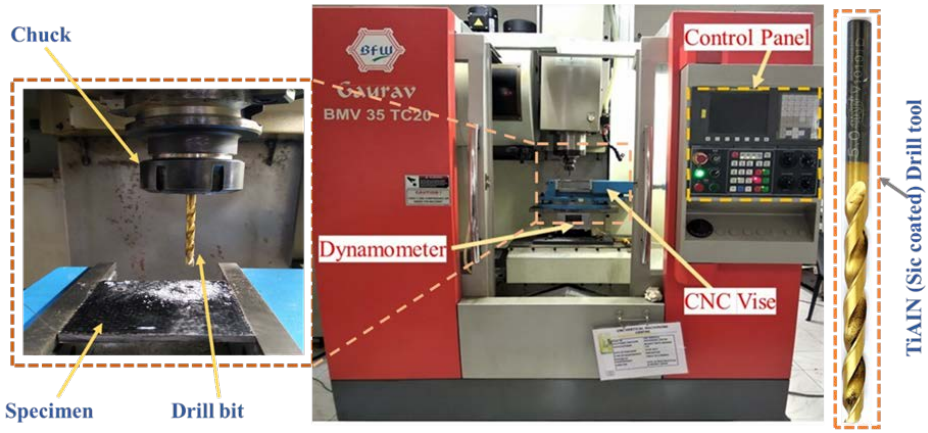

Fig. 3. Machining setup

Table 4. Specification of vertical CNC machine (BMV35 TC20)

Specifications	Value
Higher spindle speed	8,000 (10,000) rpm
Feed rates	1–10,000 mm/min
Rapid traverse X / Y / Z axes	32 / 32 / 32 m/min
Max. tool dia. with adjacent pocket full / empty	80 / 125 mm
Maximum tool weight	8 kg
Maximum tool length	200 mm
Positioning accuracy	±0.005
Clamping area	350 × 600 mm × mm
Maximum safe load on table	350 kg
Distance between table and spindle face	150–500 (350–700)

3.2. Measurement of delamination factor

The delamination failure is a significant problem in the drilling of polymer laminates. It is assessed using vision measuring equipment (model no. SDM TRZ3D) with a resolution of (0.0001 mm) and an optical magnification range of 0.7×–4.5×,

as shown in Fig. 4. As shown in Fig. 6, all the drilled hole images were captured and converted into the JPEG format by MSU-3D Pro-software. The drilling damages were measured by examining multiple spots across the drilled hole on the entry and exit sides. The delamination factor was calculated (Fig. 5) using Eq. (3).

$$\mathrm{DF} = (D_{\max}/D_0), \tag{3}$$

where DF denotes delamination factor, $D_{\max}$ is maximum damaged area around the hole periphery, and D_0 is nominal drill diameter.

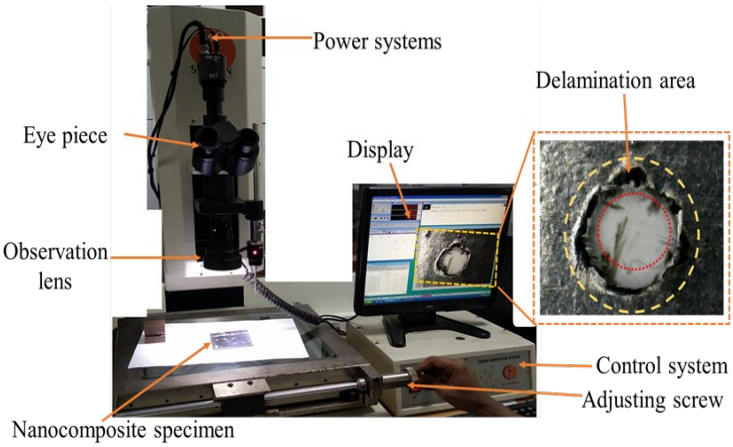

Fig. 4. Vision measurement setup

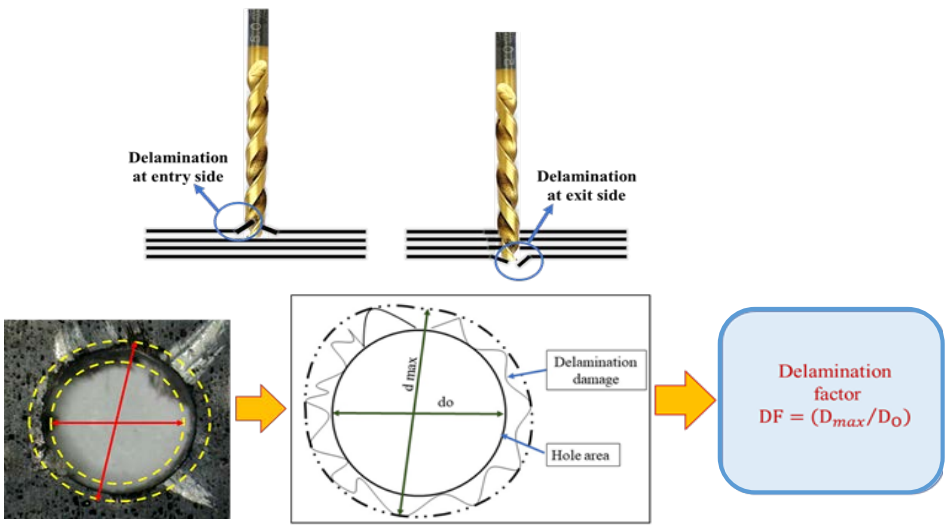

Fig. 5. Delamination mechanism and its measurement

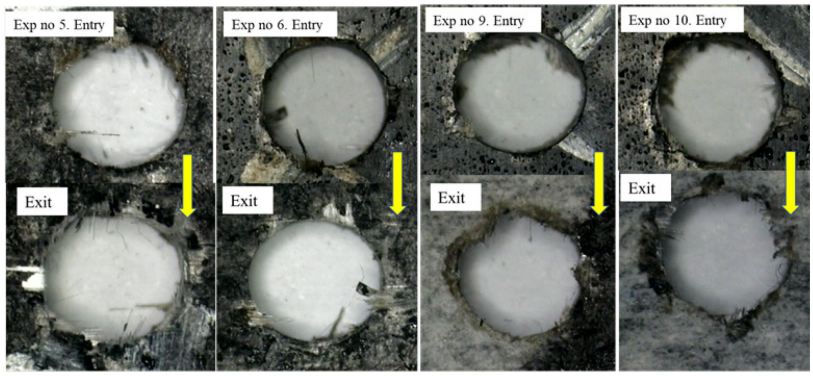

(a) 1 wt. % MWCNT incorporated GFRP/Epoxy

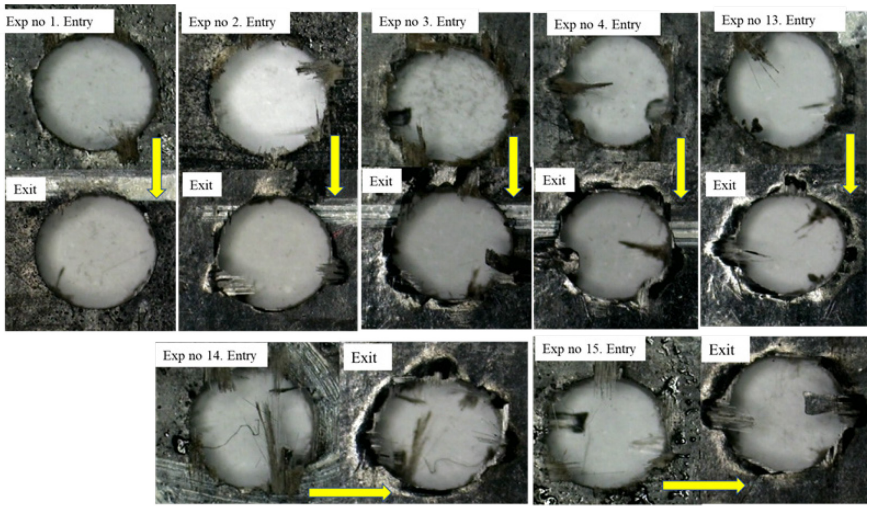

(b) 2 wt. % MWCNT incorporated GFRP/Epoxy

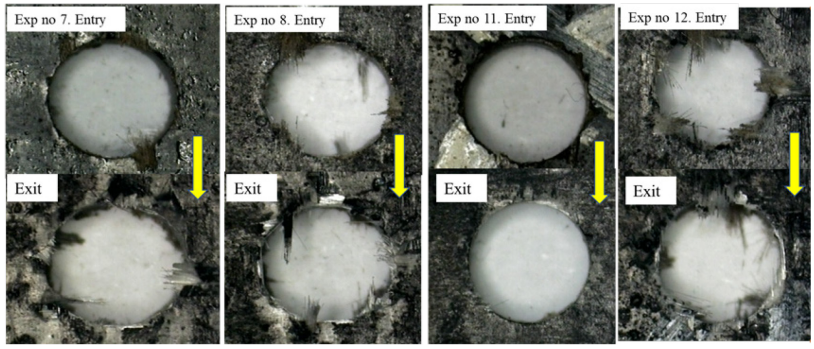

(c) 3 wt. % MWCNT incorporated GFRP/Epoxy

Fig. 6. Images of drilled holes for evaluation of delamination factor

4. Results and discussion

In the current work, fifteen experiments were performed according to the RSM theory. The TiAlN SiC coated drill bit was used for the drilling operations based on varying constraints such as the spindle speed (rpm), the feed rate (mm/min), and MWCNT wt.%. The RSM experimental design and the corresponding response values of delamination factor at entry (DF_{entry}) and exit (DF_{exit}) side, and the thrust force (Th) are given in Table 5. The ANOVA test was performed for effective assessment of the impact of drilling factors on the response. Table 6 shows the predicted and experimental response values evaluated for determining experimental accuracy. An average error of 4.272% for DF_{entry}, 3.735% for DF_{exit}, and 8.545% for Th was obtained, which signified that the developed model yielded an acceptable agreement between experimental and predicted outcomes. As evidenced by the low average error value, the proposed mathematical model of relation between variables and results can be found satisfactory.

Table 5. BBD layout and corresponding response value

Experiment No	Input parameters			Response		
	S (rpm)	F (mm/min)	wt.%	Delamination factor		Th (N)
				Entry	Exit	
1	850	85	2	1.0210	1.0367	32.97
2	2450	85	2	1.0400	1.0800	20.14
3	850	245	2	1.0706	1.0667	55.02
4	2450	245	2	1.2240	1.1450	52.78
5	850	165	1	1.0602	1.0820	55.05
6	2450	165	1	1.0432	1.0840	42.05
7	850	165	3	1.0588	1.0765	35.52
8	2450	165	3	1.2322	1.1978	30.52
9	1650	85	1	1.0008	1.1000	31.96
10	1650	245	1	1.1356	1.1398	60.75
11	1650	85	3	1.0450	1.0604	25.04
12	1650	245	3	1.2523	1.2180	50.45
13	1650	165	2	1.0045	1.0096	35.40
14	1650	165	2	1.0005	1.0056	30.79
15	1650	165	2	1.0004	1.0045	36.28

Figs. 7 to 9 display plots of the experimental outcome vs. the training outcome predicted via MINITAB software. The graphs demonstrate adequate model adequacy by showing good agreement between the experimental and predicted results. The obtained results are acceptable for an efficient drilling environment.

Table 6. Experimental outcome vs. predicted outcome and corresponding error

S. No	Experimental value			Predicted value			Error (%)		
	DF_{entry}	DF_{exit}	Th	DF_{entry}	DF_{exit}	Th	DF_{entry}	DF_{exit}	Th
1	1.021	1.037	32.97	0.966	1.020	30.17	5.366	1.616	8.491
2	1.040	1.080	20.14	1.048	1.081	21.90	0.809	0.108	8.754
3	1.071	1.067	55.02	1.110	1.093	57.39	3.693	2.470	4.313
4	1.224	1.145	52.78	1.192	1.154	49.13	2.587	0.810	6.924
5	1.060	1.082	55.05	0.995	1.038	49.82	6.186	4.054	9.506
6	1.043	1.084	42.05	1.077	1.099	41.55	3.222	1.417	1.191
7	1.059	1.077	35.52	1.082	1.075	37.75	2.166	0.153	6.269
8	1.232	1.198	30.52	1.164	1.136	29.48	5.540	5.153	3.410
9	1.001	1.100	31.96	0.964	1.032	32.07	3.702	6.164	0.350
10	1.136	1.140	60.75	1.108	1.105	59.29	2.459	3.027	2.396
11	1.045	1.060	25.04	1.051	1.069	20.00	0.562	0.803	20.121
12	1.252	1.218	50.45	1.195	1.142	47.22	4.592	6.238	6.394
13	1.005	1.010	35.4	1.079	1.087	39.65	7.444	7.677	12.000
14	1.001	1.006	30.79	1.079	1.087	39.65	7.873	8.105	28.769
15	1.000	1.005	36.28	1.079	1.087	39.65	7.884	8.224	9.283
Average error %							4.272	3.735	8.545

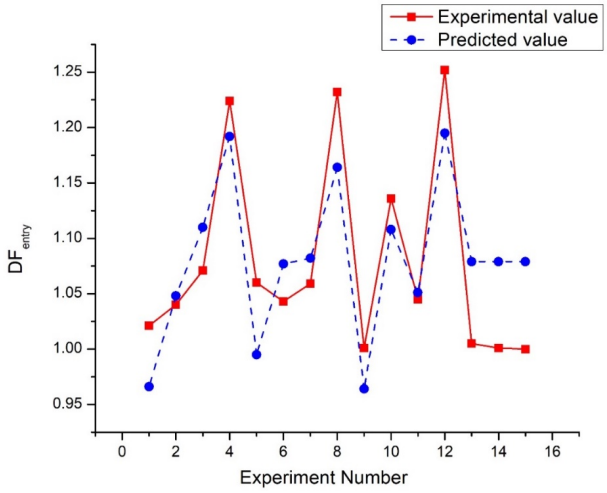

Fig. 7. Experimental vs. predicted result for DF_{entry}

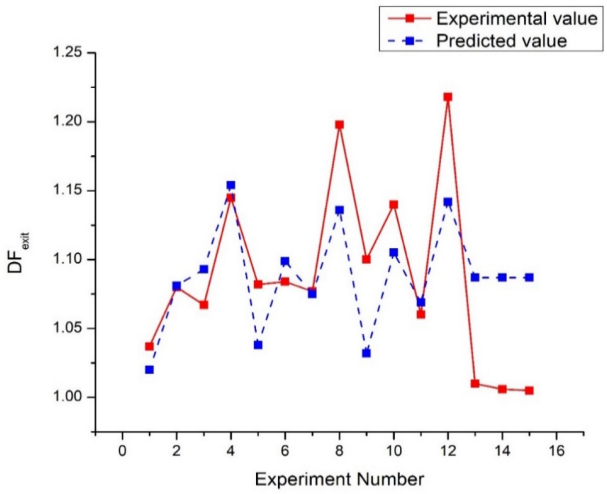

Fig. 8. Experimental vs. predicted result for DF_{entry}

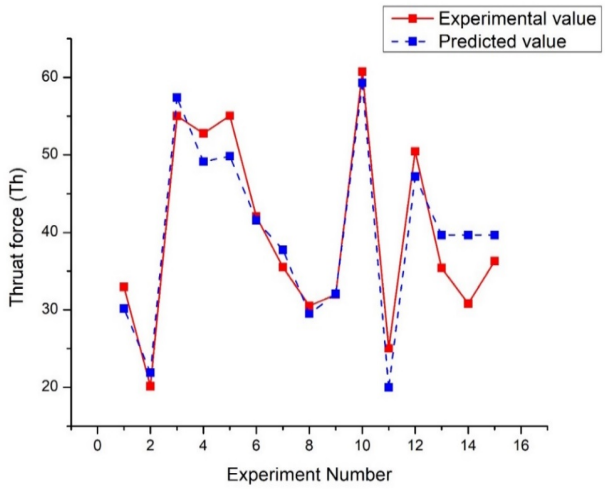

Fig. 9. Experimental vs. predicted result for thrust force (Th)

4.1. Influence of drilling parameters on DF_{entry}

The contour plots were used to illustrate the correlation between variables. In this paper, the contour plots are drawn in their respective coordinate axes, and the contour lines characterize the response factor determined through imaging processing on Minitab. Fig. 10a–10c represent the contour plot for DF_{entry} vs. feed rate and the spindle speed. Fig. 10a shows that, as the spindle speed increases, DF_{entry} decreases. It could be possible due to softening of the matrix at high cutting speeds [61].

Similarly, when the feed rate rises, DF_{entry} increases. It is evident that minimum delamination at entry appears when the speed ranges from 1000 to 2000 rpm and the feed rate is 120 to 210 mm/min. We can notice that a lower value of delamination is obtained at the combination of minimum feed rate and a relatively higher spindle speed. The higher spindle speed results in increasing temperature, which softens the matrix material, similarly, the low feed rate develops a lower cutting force. Consequently, there is little chance for delamination propagation within the matrix [62].

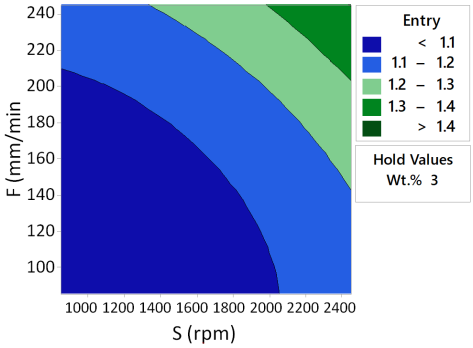

(a) Contour plot of interaction effect for spindle speed and feed rate on DF_{entry}

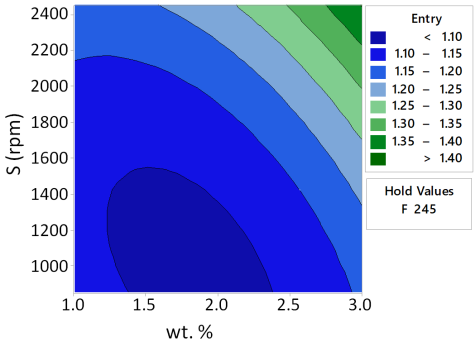

(b) Contour plot of the interaction effect of wt.% and spindle speed on DF_{entry}

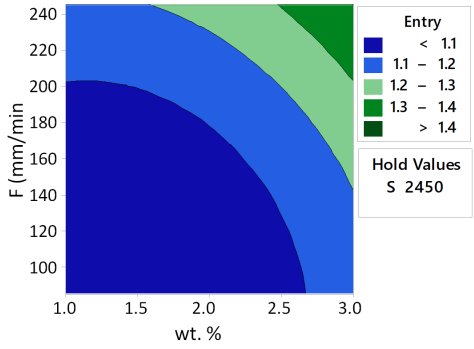

(c) Contour plot of interaction effect of wt.% and feed rate on DF_{entry}

Fig. 10. Various contour plots

Fig. 10b illustrates the interaction effect of wt.% and spindle speed on DF_{entry}. It can be observed that minimum DF_{entry} is obtained within the range of 1.4 wt.% to 2.4 wt.% and the spindle speed of 1000 rpm to near 2150. The interaction effect of wt.% and feed rate on DF_{entry} is displayed in Fig. 10c. It is noticible that the increased MWCNT wt.% raises the extent of DF_{entry}. Similarly, as the feed rate

grows from 1 to 200 mm/min, the value of DF_{entry} increases. A similar trend has been observed in previous investigations [63, 64].

In this study, ANOVA was used to estimate the impact of the linear, squared, and interaction effect of varying parameters on the delamination factor. The parameters in Table 7 are significant if $P < 0.05$. The following parameters: the spindle speed (S), the feed rate (F), wt.% of MWCNT and interactions between S and S, F and F, wt.% and wt.% and S and F, S, and wt.% are significant for the DF_{entry}, while the interaction between F and wt.% isn't. It shows that the quadratic model is the better one. The variance outcome was used to determine the model's adequacy, which is 98.54% in this case.

Table 7. ANOVA for DF_{entry}

Source	DF	Seq SS	Contribution	Adj SS	Adj MS	F-Value	P-Value
S	1	0.013514	12.30%	0.011765	0.011765	36.68	0.002^S
F	1	0.041429	37.70%	0.008021	0.008021	25.01	0.004^S
wt.%	1	0.015182	13.82%	0.016005	0.016005	49.90	0.001^S
S*S	1	0.003593	3.27%	0.005512	0.005512	17.19	0.009^S
F*F	1	0.007187	6.54%	0.008672	0.008672	27.04	0.003^S
wt.%*wt.%	1	0.012491	11.37%	0.012491	0.012491	38.95	0.002^S
S*F	1	0.004516	4.11%	0.004516	0.004516	14.08	0.013^S
S*wt.%	1	0.009063	8.25%	0.009063	0.009063	28.26	0.003^S
F*wt.%	1	0.001314	1.20%	0.001314	0.001314	4.10	0.099
Error	5	0.001604	1.46%	0.001604	0.000321		
Lack-of-Fit	3	0.001593	1.45%	0.001593	0.000531	97.05	0.010
Pure Error	2	0.000011	0.01%	0.000011	0.000005		
Total	14	0.109891	100.00%				
R^2 = 98.54%, R^2(adj) = 95.91%							
S = Significant (If $P \leq 0.05$)							

The normal probability plot for DF_{entry} is shown in Fig. 11, which illustrates the relationship between residuals and their expected values. It shows that the residuals are normally distributed. The graphs in Fig. 12 indicate that the optimal levels of parameters are: S-850, F-85, and 1 wt.% of MWCNT, which relate to the lowest delamination at entry side (DF_{entry}). Fig. 12 presents the plots of main effects of speed (S), feed rate (F), and wt.% of MWCNT on DF entry. It can be seen that the spindle speed at S-850 and the feed rate at F-85 exert the maximum effects on DF_{entry}. From Fig. 12 one can see that the maximum delamination occurrs at the highest spindle speed (S-2450), the highest feed rate (F-245), and at 3 wt.% of MWCNT. It is remarkable that the delamination factor at the entry (DF_{entry})

decreases with the decrease in the percentage of reinforcement in the material. It is primarily due to the higher feed rate creating more friction, which in turn increases the delamination factor.

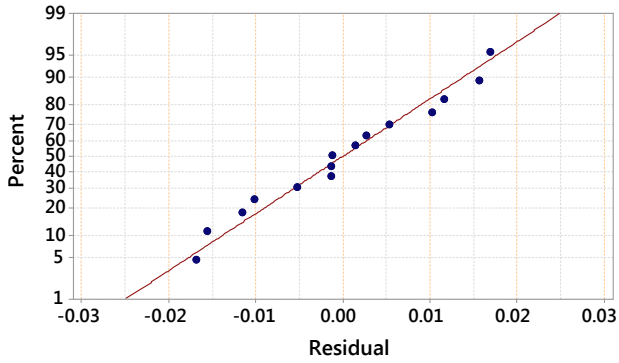

Fig. 11. Normal probability plot for DF_{entry}

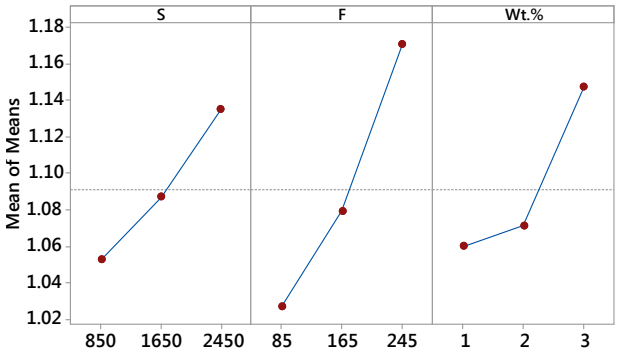

Fig. 12. Main effect plot for DF_{entry}

4.2. Influence of drilling parameters on DF_{exit}

As shown in Fig. 13, the contour plots demonstrate the interaction effect of the spindle speed S and the feed rate F on DF_{exit}. Fig. 13a depicts the contour plot for delamination factor DF_{exit} vs. F and S. As shown in the graph, when the feed rate is between 100 and 200 mm/min and the spindle speed is between 1000 and 1900 rpm, the minimum delamination factor is obtained in compared to DF_{exit} at 2400 rpm [65]. The contour plot of the interaction effect of wt.% and the spindle speed on DF_{exit} is demonstrated in Fig. 13b. The graph shows that minimum DF_{exit} is obtained in the range of 1.3 wt.% to 2.4 wt.% and the spindle speed from 1000 to near 2397 rpm. Likewise, in Fig. 13c one can observe that minimum DF_{exit} is obtained in the ranges of 1.3 to 2.5 wt.% and 120 to 180 mm/min of the feed rate.

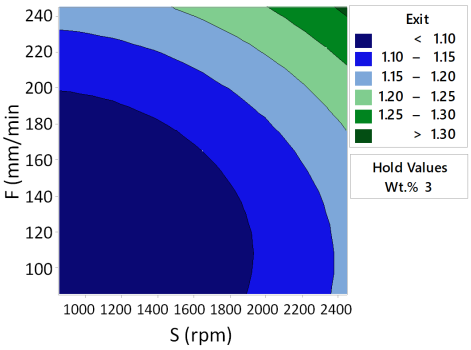

(a) Contour plot of the interaction effect of spindle speed and feed rate on DF_{exit}

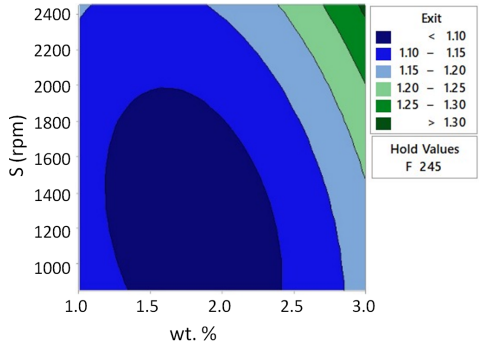

(b) Contour plot of the interaction effect of wt.% and spindle speed on DF_{exit}

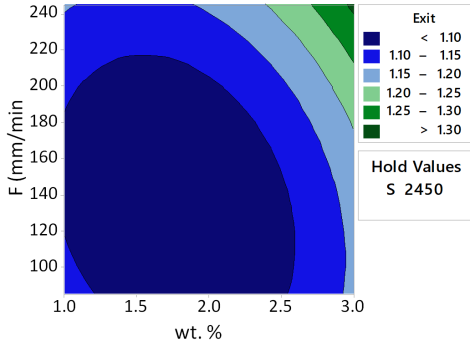

(c) Contour plot of the interaction effect of wt.% and feed rate on DF_{exit}

Fig. 13. Various contour plots

The results of variance analysis for DF_{exit} are demonstrated in Table 8 to estimate the model adequacy. The percentage contribution of the regression model (96.73%) shows that it has a significant impact on DF_{exit} with an acceptable error of (3.27%). The residuals in Fig. 14 are very close to a straight line, indicating that the errors are normally distributed. This demonstrates that the model has a high degree of fitness.

Graphs in Fig. 15 indicate that the levels of MWCNT parameters represented by S-850, F-85, and 2 wt.% produce less delamination at the exit side (DF_{exit}) than other levels of parameters. Fig. 15 depicts the main effect plots for DF_{exit}. The spindle speed of 850 rpm and the feed rate of 85 mm/min exert the maximum effects on DF_{entry}. One can also observe that maximum delamination damage is produced for S-2450, F-245, and 3 wt.% of MWCNT. The thrust force at the tool's chisel edge increases as the feed rate increases, causing delamination damage across the drilled hole surface.

Table 8. ANOVA for DF_{exit}

Source	DF	Seq SS	Contribution	Adj SS	Adj MS	F-Value	P-Value
S	1	0.007497	12.70%	0.003895	0.003895	10.08	0.025^S
F	1	0.010687	18.11%	0.008219	0.008219	21.26	0.006^S
wt.%	1	0.002697	4.57%	0.025007	0.025007	64.69	0.000^S
S*S	1	0.001383	2.34%	0.002901	0.002901	7.50	0.041^S
F*F	1	0.006458	10.94%	0.008332	0.008332	21.56	0.006^S
wt.%*wt.%	1	0.021035	35.64%	0.021035	0.021035	54.42	0.001^S
S*F	1	0.000306	0.52%	0.000306	0.000306	0.79	0.414
S*wt.%	1	0.003558	6.03%	0.003558	0.003558	9.20	0.029^S
F*wt.%	1	0.003469	5.88%	0.003469	0.003469	8.97	0.030^S
Error	5	0.001933	3.27%	0.001933	0.000387		
Lack-of-Fit	3	0.001918	3.25%	0.001918	0.000639	88.77	0.011
Pure Error	2	0.000014	0.02%	0.000014	0.000007		
Total	14	0.059024	100.00%				
R^2 = 96.73%, R^2(adj) = 90.83%, *rmS* = Significant (if P ≤ 0.05)							

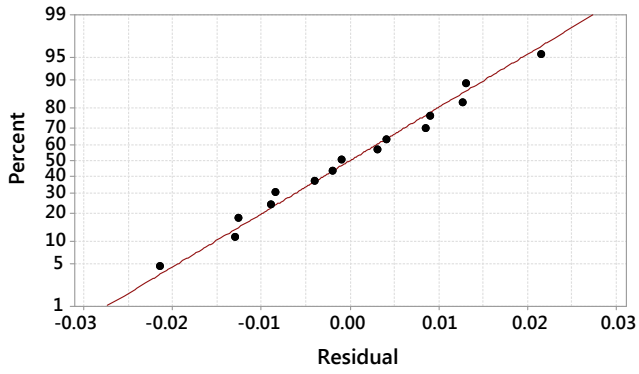

Fig. 14. Normal probability plot for DF_{exit}

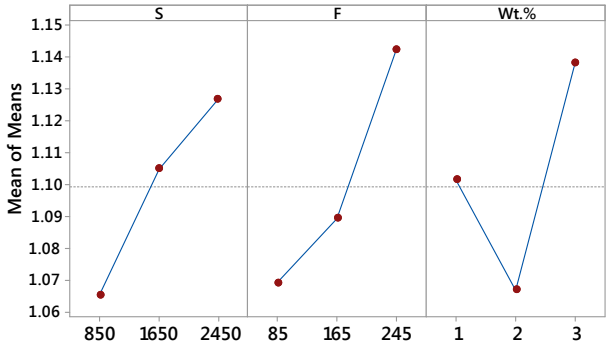

Fig. 15. Main effect plot for DF_{exit}

4.3. Influence of drilling parameters on thrust

The contour plot is demonstrated in Fig. 16 to analyze the impact of drilling factors on the thrust force (Th). Fig. 16a shows that minimum thrust force occurs at the highest spindle speed and the lowest feed rate. It can be concluded that the thrust force increases as the feed rate increases. It happens because the increasing feed rate causes a sharp rise in the feed force, resulting in a higher friction and a greater thrust force [66]. Fig. 16b shows the interaction effect of wt.% and the spindle speed on Th. It demonstrates that the minimum thrust force (Th) is obtained at the higher speeds and the lower wt.% because the contact area between reinforcement and matrix phase is growing with the increasing MWCNT wt%. Fig. 16c displays the contour plot for Th vs. F and wt.%. It is shown that the minimum thrust is obtained when wt.% ranges from 2 to 2.8 wt.% and the feed rate from 100 to 160 mm/min. It can be concluded that maximum thrust is producd as the feed rate increases, because the material puts up a greater resistance in the cutting direction in drilling of the nano-composite [63].

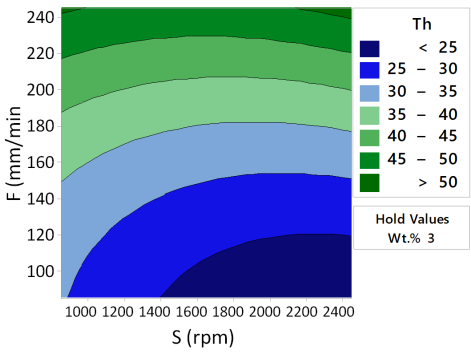

(a) Contour plot of the interaction effect of spindle speed and feed rate on Th

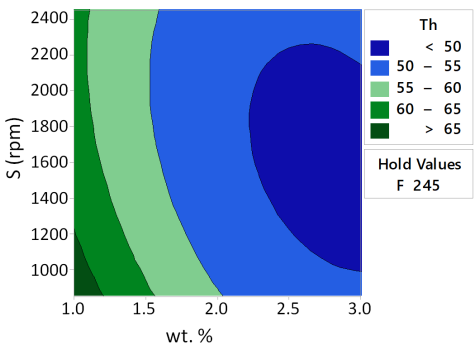

(b) Contour plot of the interaction effect of wt.% and spindle speed on Th

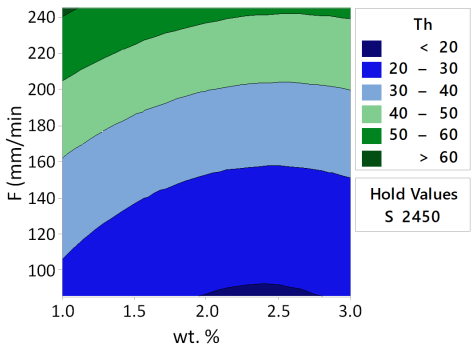

(c) Contour plot of the interaction effect of wt.% and feed rate on Th

Fig. 16. Various contour plots

The outcomes of variance analysis for thrust force (Th) are listed in Table 9. It is evident from these findings that the feed rate (F) is the most significant parameter with a 69.93% contribution. It shows that the quadratic model is the best one. The model percentage contribution shows that the regression model with R^2 = 98.00% is highly significant with an allowable error of 2.00%. The plot of the thrust force (Th) is shown in Fig. 17, demonstrating that the residuals lie near a straight line, which indicates that the errors are normally distributed.

Table 9. ANOVA for thrust (Th)

Source	DF	Seq SS	Contribution	Adj SS	Adj MS	F-Value	P-Value
S	1	136.70	6.45%	81.29	81.294	9.58	0.027^S
F	1	1482.13	69.93%	4.12	4.116	0.49	0.517^S
wt.%	1	291.37	13.75%	97.34	97.345	11.47	0.020^S
S*S	1	12.63	0.60%	21.32	21.319	2.51	0.174
F*F	1	41.51	1.96%	49.67	49.675	5.85	0.060
wt.%*wt.%	1	65.92	3.11%	65.92	65.923	7.77	0.039S
S*F	1	28.04	1.32%	28.04	28.037	3.30	0.129
S*wt.%	1	16.00	0.75%	16.00	16.000	1.89	0.228
F*wt.%	1	2.86	0.13%	2.86	2.856	0.34	0.587
Error	5	42.44	2.00%	42.44	8.487		
Lack-of-Fit	3	25.05	1.18%	25.05	8.349	0.96	0.547
Pure Error	2	17.39	0.82%	17.39	8.694		
Total	14	2119.59	100.00%				
R^2 = 98.00%, R^2(adj) = 94.39%, S = Significant (If P ≤ 0.05)							

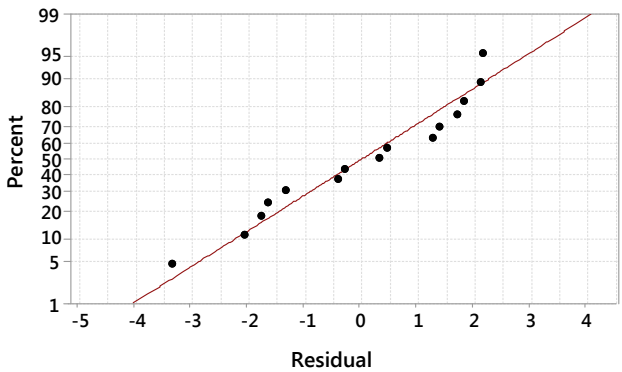

Fig. 17. Normal probability plot for Th

Fig. 18 depicts the main effects of the input factors such as speed (S), feed rate (F), and wt.% of MWCNT on the thrust force (Th) during the drilling of the nano-composite. Fig. 18 shows that the spindle speed of 2450 rpm and the feed rate of

85 mm/min exert the maximum effects on the thrust force (Th). The graphs indicate that the levels of parameters denoted as: S-2450, F-85, and 3 wt.% of MWCNT relate to the minimum thrust force, lower than that for other levels of parameters. It is also observed that maximum Th is produced for the parameter levels S-850, F-245, and 1 wt.% of MWCNT. It can be observed that the thrust force decreased as the spindle speed increases up to 2450 rpm. The increased spindle speed allows for more heat to be produced, softening the polymer matrix and decreasing the thrust force [67]. As the feed rate gradually increases, the pressure on the drill bit grows, which in turn increases the thrust force during nano-composite drilling [68, 69]. Table 10 represents a regression model of DF_{entry}, DF_{exit}, and Th, demonstrating the relationship between independent and dependent variables.

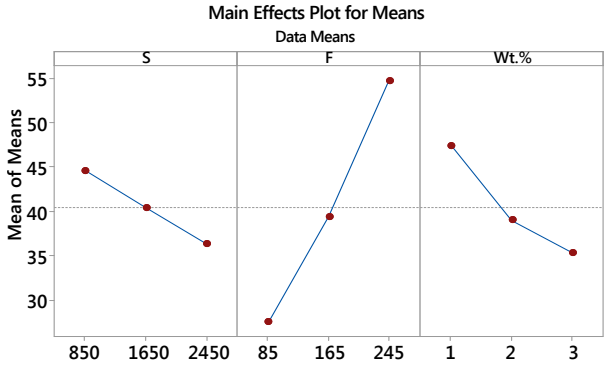

Fig. 18. Main effect plot for Th

Table 10. Regression equation for DF_{entry}, DF_{exit}, and Th

S. no.	Response	Regression equation
1	DF_{entry}	1.6987 − 0.000353 S − 0.002919 F − 0.3246 wt.% + 0.000000 S ∗ S + 0.000008 F ∗ F + 0.05816 wt.% ∗ wt.% + 0.000001 S ∗ F + 0.000060 S ∗ wt.% + 0.000227 F ∗ wt.%
2	DF_{exit}	1.736 − 0.000203 S − 0.002954 F − 0.4058 wt.% + 0.000000 S ∗ S + 0.000007 F ∗ F + 0.0755 wt.% ∗ wt.% + 0.000000 S ∗ F + 0.000037 S ∗ wt.% + 0.000368 F ∗ wt.%
3	Th	85.4 − 0.02938 S − 0.0661 F − 25.32 wt.% + 0.000004 S ∗ S + 0.000573 F ∗ F + 4.23 wt.% ∗ wt.% + 0.000041 S ∗ F + 0.00250 S ∗ wt.% − 0.0106 F ∗ wt.%

5. Control of delamination and thrust force: Grey theory

It is challenging to obtain the minimum delamination at the entry and exit sides, and a minimum thrust force while drilling the proposed nano-composites. The Grey theory is used to evaluate the optimal values of the drilling responses [70, 71].

Grey theory is a decision-making method based on the grey system theory discovered by Dr. J. Deng in 1982. Gray relational analysis (GRA) has been utilized in various scenarios to handle multiple response problems. Most previous researchers employed the Grey theory to determine the optimal condition of the output response [70, 72, 73]. In this approach, there are two zones: white and grey. The grey zone represents a system with insufficient information, whereas the white zone depicts all information. This method is used to determine the degree of association between two sequences.

The following stages are used in the Grey theory:

Step-1: Firstly, the data are normalized to avoid the variability of the experimental output, to the value range from 0 to 1. To minimize the smaller targeted value response, smaller-the-better approach is used for normalization, as in Eq. (4).

$$x_i^* = \frac{X_i(k) - \min X_i(k)}{\max x_i(k) - \min x_i(k)}\,. \tag{4}$$

For higher is better value one applies normalization using the following Eq. (5).

$$x_i^* = \frac{\max x_i(k) - x_i(k)}{\max x_i(k) - \min x_i(k)}\,, \tag{5}$$

where $i = 1, \ldots, m$; $k = 1, \ldots, n$; n represents the number of experiments, m is the number of responses. The initial series is represented by $x_i(k)$. $\max x_i(k)$ represents the biggest value, $\min x_i(k)$ indicates the lowest value, and x represents the desired value.

Step-2: The grey relational coefficient (GRC) is calculated using the following Eq. (6).

$$\gamma_i(k) = \frac{\Delta_{\min} + \gamma\Delta_{\max}}{\Delta_{oi}(k) + \gamma\Delta_{\max}}\,, \tag{6}$$

where Δ_{oi}, represent the deviation sequence:

$$\Delta_{oi} = |x_o(k) - x_i(k)|\,, \tag{7}$$

where $x_o(k)$ represent the reference sequence and $x_i(k)$ represent a comparability sequence. $\Delta_{\min}$ represent the minimum and $\Delta_{\max}$ is the maximum values of the absolute differences between all comparison sequences.

Step-3: The grey relational grade (GRG) is calculated by averaging the GRC values. The GRG value is calculated using the following Eq. (8).

$$G_i = \frac{1}{n}\sum_{k=1}^{n}\gamma_i(k)\,, \tag{8}$$

where, G_i represent the required grade value and n is the number of responses.

The experiment data (Table 11) are aggregated into a single grey relational grade (GRG). The optimal combinations, according to the Grey theory, are observed

for S (1650 Level-2), F (165 Level-2), and 2 wt.% of MWCNT (Level-2), as shown in Table 11. The lower value of the decreased DF_{entry}, DF_{exit}, and Th is determined by the Grey technique. The GRG graph and the mean table estimate the effect of the drilling parameter. The ANOVA is employed to examine the impact of the drilling factors on GRG. It is shown that the feed rate is the most significant factor affecting the value of the objective function (Table 12).

Table 11. Response table for GRA

Level	Factor			GRG
	S	F	wt. %	
L1	0.519	0.670	0.480	0.881
L2	0.541	0.529	0.590	
L3	0.471	0.335	0.448	
Max. value	0.541	0.670	0.590	
Optimal setting	1650	165	2	

Table 12. ANOVA for GRG

Source	DF	Seq SS	Contribution	Adj SS	Adj MS	F-Value	P-Value
S	1	0.004544	0.86%	0.094208	0.094208	184.21	0.000^S
F	1	0.225504	42.61%	0.039232	0.039232	76.71	0.000^S
wt.%	1	0.002020	0.38%	0.140131	0.140131	274.00	0.000^S
S*S	1	0.057553	10.88%	0.081695	0.081695	159.74	0.000^S
F*F	1	0.051405	9.71%	0.066127	0.066127	129.30	0.000^S
wt.%*wt.%	1	0.163432	30.88%	0.163432	0.163432	319.56	0.000^S
S*F	1	0.010547	1.99%	0.010547	0.010547	20.62	0.006^S
S*wt.%	1	0.010929	2.07%	0.010929	0.010929	21.37	0.006^S
F*wt.%	1	0.000694	0.13%	0.000694	0.000694	1.36	0.297
Error	5	0.002557	0.48%	0.002557	0.000511		
Lack-of-Fit	3	0.000600	0.11%	0.000600	0.000200	0.20	0.886
Pure error	2	0.001958	0.37%	0.001958	0.000979		
Total	14	0.529185	100.00%				
R^2 = 99.52%, R^2(adj) = 98.65% S = Significant (if P ≤ 0.05)							

GRG regression equations obtained here also follow the mathematical model, as discussed earlier in section 5. The regression model exhibits a high fitness with R^2 and R^2(adj) values of 99.52% and 98.65%, respectively (Table 13). The

optimal condition obtained from the Grey theory is S2F2 wt.%.2. The graph of the GRG highest value in Fig. 19 shows the feasible experiment for optimal response value.

Table 13. The regression equation for GRG

Response	Regression equation
GRG	$-1.288 + 0.001000\,S + 0.006455\,F + 0.9606\,wt.\% - 0.000000\,S * S - 0.000021\,F * F - 0.2104\,wt.\% * wt.\% - 0.000001\,S * F - 0.000065\,S * wt.\% - 0.000165\,F * wt.\%$

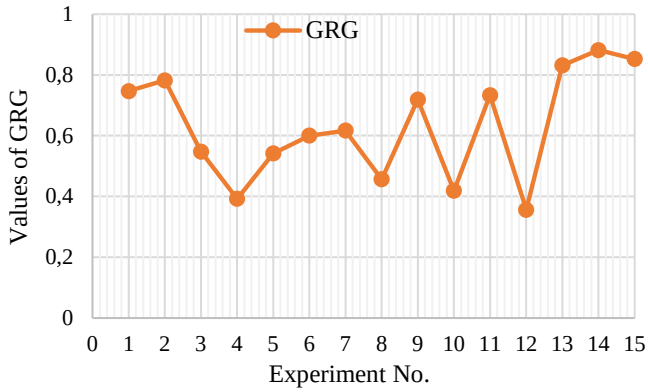

Fig. 19. GRG graph

6. Microstructural investigation of machined surface

Scanning electron microscope (SEM) micrographs were utilized to evaluate the drilled hole surface quality (Fig. 20). SEM analysis was performed on the cut section of the drilled hole in the optimal conditions (Exp. no. 11) to assess the machined surface quality [74]. The SEM image shows the push-out delamination mechanism associated with the thrust force, the laminate interface accuracy, and the process conditions. When the drill tool inter in the composite the uncute layer become more sensitive to deform hole which causes delamination. Fig. 20 also shows a good surface finishing of the workpiece's cut surface. It also demonstrates that the higher feed rate and the increased fiber orientation angle cause a greater delamination on the exit side than on the entry side [75, 76]. The higher spindle speed improves the machined surface quality by reducing material deformation at the tool-chip contact during the cutting process, which results in a better surface. Further, the improved surface obtained thanks to the decreased feed rate could be attributed to the composite material's lower strain rate, resulting in a reduced nano-composite breaking [77, 78].

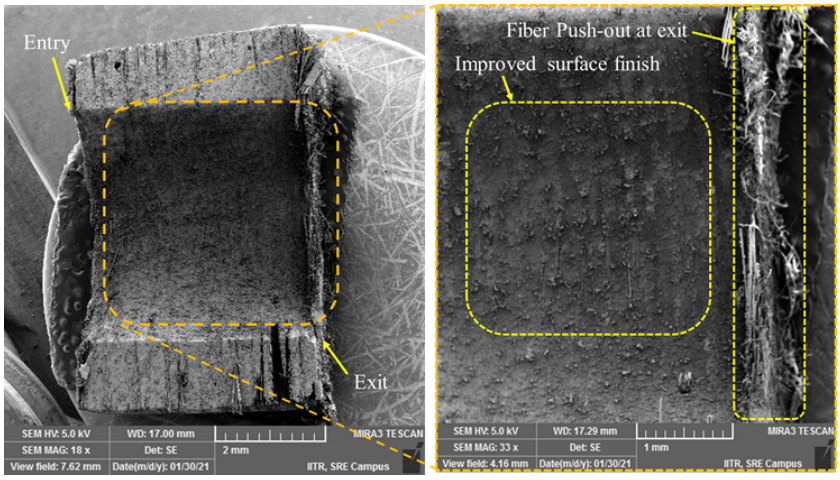

Fig. 20. SEM of the drilled hole

7. Conclusion

This paper presents the measurement and control of the delamination at the entry and exit side, and the thrust force generation during drilling of polymer nano-composites modified by MWCNT and glass fiber. The variance analysis shows the effect of parameters (S, F, and wt.% of MWCNT) on the drilling responses. The regression model is created, and validation tests are performed to ensure that the model is correct. The conclusions drawn from this study are the following:

- The created RSM-based model makes it possible to assess delamination and thrust in drilling MWCNT incorporate GFRP/epoxy nano-composites. The ANOVA results revealed that spindle speed and feed rate were the two vital factors influencing the quality of the machined holes in nano-composites.
- ANOVA results demonstrate that the derived quadratic regression model of DF_{entry}, DF_{exit}, and Th provides a good relationship for performing the experimentation and response prediction. The model adequacy coefficients (R^2 values) of DF_{entry}, DF_{exit}, and Th are 98.54%, 96.73%, and 98.80%, respectively.
- The GRA optimization technique reveals that the feed rate substantially affects delamination since the thrust force varies with the feed rate. The regression model of GRG exhibits a high degree of fitness with R^2 = 99.52%, and R^2(adj) = 98.65%.
- Confirmation experiments show that there is a very minimal error associated with the thrust force. The results of Grey optimization demonstrate a promising improvement in the response value. This confirms the drilling machinability of the proposed nano-composites.

- SEM images are used to investigate the morphology of the drilled surface. TiAIN Sic coated drills tool produces high-quality machined surfaces during the drilling of epoxy nano-composites.

The MWCNT reinforced glass fiber reinforced polymer nano-composite is a promising and economical substitute for a conventional material due to its outstanding properties. The machinability-related studies of such a composite provide an insight into selecting optimal process parameters for an efficient machining environment. The developed optimization tool shows a good applicability for optimizing machining parameters for a composite material. Therefore, it can be customized for further studies in an extended range of process parameters such as tool design, analysis of temperature between machining interfaces, tool wear, chips formation, etc. The extensive research on the proposed MWCNT/GFRP nano-composites could provide polymer manufacturers with a cost-effective and efficient machining solution.

Acknowledgements

The authors would like to acknowledge the kind support of the Ministry of Textiles, Govt. of India, New Delhi, India, to extend all possible help in carrying out this research work directly or indirectly.

References

[1] J. Du, H. Zhang, Y. Geng, W. Ming, W. He, J. Ma, Y. Cao, X. Li, and K. Liu. A review on machining of carbon fiber reinforced ceramic matrix composites. *Ceramics International*, 45(15):18155–18166, 2019. doi: 10.1016/j.ceramint.2019.06.112.

[2] N.R.M. Akmam, M. Mullah, and M.Z. Zakaria. Study on tool wear mechanism during milling of JFRP composite. *International Journal of Science and Engineering Investigations*, 9(98):20–26, 2020.

[3] D. Geng, Y. Liu, Z. Shao, Z. Lu, J. Cai, X. Li, X. Jiang, and D. Zhang. Delamination formation, evaluation and suppression during drilling of composite laminates: A review. *Composite Structures*, 216:168–86, 2019. doi: 10.1016/j.compstruct.2019.02.099.

[4] G. Rajaraman, S.K. Agasti, and M.P. Jenarthanan. Investigation on effect of process parameters on delamination during drilling of kenaf-banana fiber reinforced in epoxy hybrid composite using Taguchi method. *Polymer Composites*, 41(3):994–1002, 2020. doi: 10.1002/pc.25431.

[5] M. Ramesh and A. Gopinath. Measurement and analysis of thrust force in drilling sisal-glass fiber reinforced polymer composites. *IOP Conference Series: Materials Science and Enginierring*, 197:012056, 2017. doi: 10.1088/1757-899X/197/1/012056.

[6] U.H. Babu, N.V. Sai, and R.K. Sahu. Artificial intelligence system approach for optimization of drilling parameters of glass-carbon fiber/polymer composites. *Silicon*, 13:2943–2957, 2021. doi: 10.1007/s12633-020-00637-5.

[7] W. Li, A. Dichiara, and J. Bai. Carbon nanotube-graphene nanoplatelet hybrids as high-performance multifunctional reinforcements in epoxy composites. *Composites Science and Technology*, 74:221–227, 2013. doi: 10.1016/j.compscitech.2012.11.015.

[8] S.G. Ghalme, Y. Bhalerao, and K. Phapale. Analysis of factors affecting delamination in drilling GFRP composite. *Journal of Computational and Applied Research in Mechanical Engineering*, 10(2):281–289, 2021. doi: 10.22061/jcarme.2019.4397.1530.

[9] S. Manteghi, A. Sarwar, Z. Fawaz, R. Zdero, and H. Bougherara. Mechanical characterization of the static and fatigue compressive properties of a new glass/flax/epoxy composite material using digital image correlation, thermographic stress analysis, and conventional mechanical testing. *Materials Science and Engineering: C*, 99:940–950, 2019. doi: 10.1016/j.msec.2019.02.041.

[10] J. Samuel, A. Dikshit, R.E. DeVor, S.G. Kapoor, and K.J. Hsia. Effect of carbon nanotube (CNT) loading on the thermomechanical properties and the machinability of CNT-reinforced polymer composites. *Journal of Manufacturing Science and Engineering*, 131(3):031008, 2009. doi: 10.1115/1.3123337.

[11] A. Babu Arumugam, V. Rajamohan, N. Bandaru, E.P. Sudhagar, and S.G. Kumbhar. Vibration analysis of a carbon nanotube reinforced uniform and tapered composite beams. *Archives of Acoustics*, 44(2):309–320. doi: 10.24425/aoa.2019.128494.

[12] X. Wang, Q. Zheng, S. Dong, A. Ashour, and B. Han. Interfacial characteristics of nano-engineered concrete composites. *Construction and Building Matererials*, 259:119803, 2020. doi: 10.1016/j.conbuildmat.2020.119803.

[13] A.K. Chakraborty, T. Plyhm, M. Barbezat, A. Necola, and G.P. Terrasi. Carbon nanotube (CNT)-epoxy nanocomposites: A systematic investigation of CNT dispersion. *Journal of Nanoparticle Research*, 13:6493–6506, 2011. doi: 10.1007/s11051-011-0552-3.

[14] D.K. Rathore, R.K. Prusty, D.S. Kumar, and B.C. Ray. Mechanical performance of CNT-filled glass fiber/epoxy composite in in-situ elevated temperature environments emphasizing the role of CNT content. *Composites Part A: Applied Science and Manufacturing*, 84:364–376, 2016. doi: 10.1016/j.compositesa.2016.02.020.

[15] L. Sun, Y. Zhao, Y. Duan , and Z. Zhang. Interlaminar shear property of modified glass fiber-reinforced polymer with different MWCNTs. *Chinese Journal of Aeronautics*, 21(4):361–369, 2008. doi: 10.1016/S1000-9361(08)60047-3.

[16] A. Esmaeili, C. Sbarufatti, andA.M.S. Hamouda. Investigation of mechanical properties of MWCNTs doped epoxy nanocomposites in tensile, fracture and impact tests. *Materials Science Forum*, 990:239–243, 2020. doi: 10.4028/www.scientific.net/msf.990.239.

[17] A. Tabatabaeian and A.R. Ghasemi. The impact of MWCNT modification on the structural performance of polymeric composite profiles. *Polymer Bulletin*, 77:6563–6576, 2020. doi: 10.1007/s00289-019-03088-0.

[18] A. Gaurav and K.K. Singh. Effect of pristine MWCNTs on the fatigue life of GFRP laminates-an experimental and statistical evaluation. *Composites Part B: Engineering*, 172:83–96, 2019. doi: 10.1016/j.compositesb.2019.05.069.

[19] B. Shivamurthy, S. Anandhan, K.U. Bhat, and B.H.S. Thimmappa. Structure-property relationship of glass fabric/MWCNT/epoxy multi-layered laminates. *Composites Communications*, 22:100460, 2020. doi: 10.1016/j.coco.2020.100460.

[20] A. Uysal. Evaluation of drilling parameters on surface roughness and burr when drilling carbon black reinforced high-density polyethylene. *Journal of Composite Materials*, 52(20): 2719–2727, 2018. doi: 10.1177/0021998317752505.

[21] F. Susac and F. Stan. Experimental investigation, modeling and optimization of circularity, cylindricity and surface roughness in drilling of PMMA using ANN and ANOVA. *Materiale Plastice*, 57(1):57–68, 2020. doi: 10.37358/MP.20.1.5312.

[22] P. Czarnocki and T. Zagrajek. Growth stability analysis of embedded delaminations with the use of FE node relocation procedure and effective resistance curve concept. *Archive of Mechanical Engineering*, 67(4):415–433, 2020. doi: 10.24425/ame.2020.131702.

[23] L. Liu, C. Qi, F. Wu, X. Zhang, and X. Zhu. Analysis of thrust force and delamination in drilling GFRP composites with candle stick drills. *The International Journal of Advanced Manufacturing Technology*, 95:2585–2600, 2018. doi: 10.1007/s00170-017-1369-8.

[24] M.P. Jenarthanan and R. Jeyapaul. Optimisation of machining parameters on milling of GFRP composites by desirability function analysis using Taguchi method. *International Journal of Engineering, Science and Technology*, 5(4):23–36. doi: 10.4314/ijest.v5i4.3.

[25] P. Raveendran and P. Marimuthu. Multi-response optimization of turning parameters for machining glass fiber-reinforced plastic composite rod. *Advances in Mechanical Engineering*, 7:1–10, 2015. doi: 10.1177/1687814015620109.

[26] D.I. Poór, N. Geier, C. Pereszlai, and J. Xu. A critical review of the drilling of CFRP composites: Burr formation, characterisation and challenges. *Composites Part B: Engineering*, 223:109155, 2021. doi: 10.1016/j.compositesb.2021.109155.

[27] R. Higuchi, S. Warabi, W. Ishibashi, and T. Okabe. Experimental and numerical investigations on push-out delamination in drilling of composite laminates. *Composites Science and Technology*, 198:108238, 2020. doi: 10.1016/j.compscitech.2020.108238.

[28] J. Kumar, R.K. Verma, and A.K. Mondal. Predictive modeling and machining performance optimization during drilling of polymer nanocomposites reinforced by graphene oxide/carbon fiber. *Archive of Mechanical Engineering*, 67(2):229–258. doi: 10.24425/ame.2020.131692.

[29] N. Hoffmann, G.S.C. Souza, A.J. Souza, and V. Tita. Delamination and hole wall roughness evaluation in air-cooled drilling of carbon fiber-reinforced polymer. *Journal of Composite Materials*, 55(23):3161–3174, 2021. doi: 10.1177/00219983211009281.

[30] A.T. Erturk, F. Vatansever, E. Yarar, E.A. Guven, and T. Sinmazcelik. Effects of cutting temperature and process optimization in drilling of GFRP composites. *Journal of Composite Materials*, 55(2):235–249, 2021. doi: 10.1177/0021998320947143.

[31] R. Pramod, S. Basavarajappa, G.B. Veeresh Kumar, and M. Chavali. Drilling induced delamination assessment of nanoparticles reinforced polymer matrix composites.*Proceedings of the Institution of Mechanical Engineers, Part C: Journal of Mechanical Engineering Science*, 2021. doi: 10.1177/09544062211030967.

[32] P.K. Kharwar, R.K. Verma, N.K. Mandal, and A.K. Mondal. Swarm intelligence integrated approach for experimental investigation in milling of multiwall carbon nanotube/polymer nanocomposites. *Archive of Mechanical Engineering*, 67(3):353–376, 2020. doi: 10.24425/ame.2020.131698.

[33] S. Gokulkumar, P.R. Thyla, R. ArunRamnath, and N. Karthi. Acoustical analysis and drilling process optimization of Camellia Sinensis / Ananas Comosus / GFRP / Epoxy composites by TOPSIS for indoor applications. *Journal of Natural Fibers*, 18(12):2284–2301. doi: 10.1080/15440478.2020.1726240.

[34] S. Liu, T. Yang, C. Liu, Y. Jin, D. Sun, and Y. Shen. Modelling and experimental validation on drilling delamination of aramid fiber reinforced plastic composites. *Composite Structures*, 236:111907, 2020. doi: 10.1016/j.compstruct.2020.111907.

[35] U. Bhushi, J. Suthar, and S.N. Teli. Performance analysis of metaheuristics optimization techniques for drilling process on CFRP composites.*Materials Today: Proceedings*, 28(2):1106–1114, 2020. doi: 10.1016/j.matpr.2020.01.091.

[36] A. Janakiraman, S. Pemmasani, S. Sheth, C. Kannan, and A.S.S. Balan. Experimental investigation and parametric optimization on hole quality assessment during drilling of CFRP/GFRP/Al stacks. *Journal of The Institution of Engineers (India): Series C*, 101:291–302, 2020. doi: 10.1007/s40032-020-00563-w.

[37] M. Mudhukrishnan, P. Hariharan, and K. Palanikumar. Measurement and analysis of thrust force and delamination in drilling glass fiber reinforced polypropylene composites using different drills. *Measurement*, 149:106973, 2020. doi: 10.1016/j.measurement.2019.106973.

[38] B.-C. Kwon, N.D.D. Mai, E.S. Cheon, and S.L. Ko. Development of a step drill for minimization of delamination and uncut in drilling carbon fiber reinforced plastics (CFRP). *The International Journal of Advanced Manufacturing Technology* , 106:1291–1301, 2020. doi: 10.1007/s00170-019-04423-5.

[39] T. Panneerselvam, S. Raghuraman, T.K. Kandavel, and K. Mahalingam. Evaluation and analysis of delamination during drilling on Sisal-Glass Fibres Reinforced Polymer. *Measurement*, 154:107462, 2020. doi: 10.1016/j.measurement.2019.107462.

[40] A. Landesmann, C.A. Seruti, and E. de Miranda Batista. Mechanical properties of glass fiber reinforced polymers members for structural applications. *Materials Research*, 18(6):1372–1383, 2015. doi: 10.1590/1516-1439.044615.

[41] K. Askaripour and A. Zak. A survey of scrutinizing delaminated composites via various categories of sensing apparatus. *Journal of Composites Science*, 3(4):95, 2019 doi: 10.3390/jcs3040095.

[42] M.R. Sanjay and B. Yogesha. Studies on natural/glass fiber reinforced polymer hybrid composites: An evolution. *Materials Today: Proceedings*, 4(2):2739–2747, 2017. doi: 10.1016/j.matpr.2017.02.151.

[43] M.Y. Abdellah, M.S. Alsoufi, M.K. Hassan,H.A. Ghulman, and A.F. Mohamed. Extended finite element numerical analysis of scale effect in notched glass fiber reinforced epoxy composite. *Archive of Mechanical Engineering*, 62(2):217–236, 2015. doi: 10.1515/meceng-2015-0013.

[44] K. Rodsin, Q. Hussain, P. Joyklad, A. Nawaz, and H. Fazliani. Seismic strengthening of non-ductile bridge piers using low-cost glass fiber polymers. B*Bulletin of the Polish Academy of Sciences: Technical Sciences*, 68(6):1457–1470, 2020. doi: 10.24425/bpasts.2020.135383.

[45] R. Bielawski, M. Kowalik, K. Suprynowicz, R. Rządkowski,and P. Pyrzanowski. Experimental study on the riveted joints in glass fibre reinforced plastics (GFRP). *Archive of Mechanical Engineering*, 64(3):301–313, 2017. doi: 10.1515/meceng-2017-0018.

[46] N. Rasana, K. Jayanarayanan, B.D.S. Deeraj, and K. Joseph. The thermal degradation and dynamic mechanical properties modeling of MWCNT/glass fiber multiscale filler reinforced polypropylene composites. *Composites Science and Technology*, 169:249–259, 2019. doi: 10.1016/j.compscitech.2018.11.027.

[47] A.D. Dobrzańska-Danikiewicz, D. Łukowiec, D. Cichocki, and W. Wolany. Comparison of the MWCNTs-Rh and MWCNTs-Re carbon-metal nanocomposites obtained in hightemperature. *Archives of Metallurgy and Materials*, 60(3):2053–2060, 2015. doi: 10.1515/amm-2015-0348.

[48] Ö Demircan, K. Kadıoğlu, P. Çolak, E. Günaydın, M. Doğu, N. Topalömer, and V. Eskizeybekl. Compression after impact and Charpy impact characterizations of glass fiber/epoxy/MWCNT composites. *Fibers and Polymers*, 21(8):1824–1831, 2020. doi: 10.1007/s12221-020-9921-9.

[49] P.K. Kharwar and R.K. Verma. Machining performance optimization in drilling of multiwall carbon nano tube /epoxy nanocomposites using GRA-PCA hybrid approach. *Measurement*, 158:107701, 2020. doi: 10.1016/j.measurement.2020.107701.

[50] C.R.Raajeshkrishna, P. Chandramohan, and V.S. Saravanan. Thermomechanical characterization and morphological analysis of nano basalt reinforced epoxy nanocomposites. *International Journal of Polymer Analysis and Characterization*, 25(4):216–226, 2020. doi: 10.1080/1023666X.2020.1781479.

[51] K.M. Tripathi, A. Sachan, M. Castro, V. Choudhary, S.K. Sonkar, and J.F. FellerF. Green carbon nanostructured quantum resistive sensors to detect volatile biomarkers. *Sustainable Materials and Technologies*, 16:1–11, 2018. doi: 10.1016/j.susmat.2018.01.001.

[52] P. Rawat and K.K. Singh. A strategy for enhancing shear strength and bending strength of FRP laminate using MWCNTs. *IOP Conference Series: Materials Science and Engineering*, 149:012105, 2015. doi: 10.1088/1757-899X/149/1/012105.

[53] S. Yeasmin, J.H. Yeum, and S.B Yang. Fabrication and characterization of pullulan-based nanocomposites reinforced with montmorillonite and tempo cellulose nanofibril. *Carbohydrate Polymers*, 240:116307, 2020. doi: 10.1016/j.carbpol.2020.116307.

[54] K. Hosseinpour and A.R. Ghasemi. Agglomeration and aspect ratio effects on the long-term creep of carbon nanotubes/fiber/polymer composite cylindrical shells. *Journal of Sandwich Structures & Materials*, 23(4):1272–1291, 2021. doi: 10.1177/1099636219857200.

[55] A.R. Ghasemi, M. Mohandes, R. Dimitri, and F. Tornabene. Agglomeration effects on the vibrations of CNTs/fiber/polymer/metal hybrid laminates cylindrical shell. *Composites Part B: Engineering*, 167:700–716, 2019. doi: 10.1016/j.compositesb.2019.03.028.

[56] G.C. Onwubolu and S. Kumar. Response surface methodology-based approach to CNC drilling operations.*Journal of Materials Processing Technology*, 171(1):41–47, 2006. doi: 10.1016/j.jmatprotec.2005.06.064.

[57] E. Kilickap, M. Huseyinoglu, and A. Yardimeden. Optimization of drilling parameters on surface roughness in drilling of AISI 1045 using response surface methodology and genetic algorithm.*The International Journal of Advanced Manufacturing Technology*, 52:79–88, 2011. doi: 10.1007/s00170-010-2710-7.

[58] C.C. Tsao. Comparison between response surface methodology and radial basis function network for core-center drill in drilling composite materials. *The International Journal of Advanced Manufacturing Technology*, 37:1061–1068, 2008. doi: 10.1007/s00170-007-1057-1.

[59] E. Kilickap. Modeling and optimization of burr height in drilling of Al-7075 using Taguchi method and response surface methodology. *The International Journal of Advanced Manufacturing Technology*, 49:911–923, 2010. doi: 10.1007/s00170-009-2469-x.

[60] A. Ramaswamy and A.V. Perumal. Multi-objective optimization of drilling EDM process parameters of LM13 Al alloy–10ZrB_2–5TiC hybrid composite using RSM. *Journal of the Brazilian Society of Mechanical Sciences and Engineering*, 42:432, 2020. doi: 10.1007/s40430-020-02518-9.

[61] K.K. Panchagnula and K. Palaniyandi. Drilling on fiber reinforced polymer/nanopolymer composite laminates: A review. *Journal of Materials Research and Technology*, 7(2):180–189, 2018. doi: 10.1016/j.jmrt.2017.06.003.

[62] D. Kumar and K.K. Singh. An experimental investigation of surface roughness in the drilling of MWCNT doped carbon/epoxy polymeric composite material. *IOP Conference Series: Materials Science and Engineering*, 149:012096, 2016. doi: 10.1088/1757-899X/149/1/012096.

[63] M. Mudegowdar. Influence of cutting parameters during drilling of filled glass fabric-reinforced epoxy composites. *Science and Engineering of Composite Materials*, 22(1):81–88, 2013. doi: 10.1515/secm-2013-0198.

[64] Ş Bayraktar and Y. Turgut. Determination of delamination in drilling of carbon fiber reinforced carbon matrix composites/Al 6013-T651 stacks. *Measurement*, 154:107493, 2020. doi: 10.1016/j.measurement.2020.107493.

[65] K.M. John and T.S. Kumaran. Backup support technique towards damage-free drilling of composite materials: A review. *International Journal of Lightweight Materials and Manufacture*, 3(4):357–364, 2020. doi: 10.1016/j.ijlmm.2020.06.001.

[66] L.M.P. Durão, J.M.R.S. Tavares, V.H.C. De Albuquerque, J.F.S. Marques, and O.N.G. Andrade. Drilling damage in composite material. *Materials*, 7(5):3802–3819, 2014. doi: 10.3390/ma7053802.

[67] B.R.N. Murthy, R. Beedu, R. Bhat, N. Naik, and P. Prabakar. Delamination assessment in drilling basalt/carbon fiber reinforced epoxy composite material. *Journal of Materials Research and Technology*, 9(4):7427–7433, 2020. doi: 10.1016/j.jmrt.2020.05.001.

[68] S.O. Ojo, S.O. Ismail, M. Paggi, and H.N. Dhakal. A new analytical critical thrust force model for delamination analysis of laminated composites during drilling operation. *Composites Part B: Engineering*, 124:207–217, 2017. doi: 10.1016/j.compositesb.2017.05.039.

[69] D. Wang, F. Jiao, and X. Mao. Mechanics of thrust force on chisel edge in carbon fiber reinforced polymer (CFRP) drilling based on bending failure theory. *International Journal of Mechanical Sciences*, 169:105336, 2020. doi: 10.1016/j.ijmecsci.2019.105336.

[70] N. Kaushik and S. Singhal. Hybrid combination of Taguchi-GRA-PCA for optimization of wear behavior in AA6063/SiC_p matrix composite. *Production & Manufacturing Research* , 6(1):171–189, 2018. doi: 10.1080/21693277.2018.1479666.

[71] K. Aslantas, E. Ekici, and A. Çiçek. Optimization of process parameters for micro milling of Ti-6Al-4V alloy using Taguchi-based gray relational analysis. *Measurement*, 128:419–427, 2018. doi: 10.1016/j.measurement.2018.06.066.

[72] S. Ragunath, C. Velmurugan, and T. Kannan. Optimization of drilling delamination behavior of GFRP/clay nano-composites using RSM and GRA methods. *Fibers and Polymers*, 18:2400–2409, 2017. doi: 10.1007/s12221-017-7420-4.

[73] P.M. Gopal and K. Soorya Prakash. Minimization of cutting force, temperature and surface roughness through GRA, TOPSIS and Taguchi techniques in end milling of Mg hybrid MMC. *Measurement*, 116:178–192, 2018. doi: 10.1016/j.measurement.2017.11.011.

[74] S.M. Shahabaz, N. Shetty, S.D. Shetty, and S.S. Sharma. Surface roughness analysis in the drilling of carbon fiber/epoxy composite laminates using hybrid Taguchi-Response experimental design. *Materials Research Express*, 7(1):015322, 2020. doi: 10.1088/2053-1591/ab6198.

[75] D. Kumar, K.K. Singh, and R. Zitoune. Experimental investigation of delamination and surface roughness in the drilling of GFRP composite material with different drills. *Advanced Manufacturing: Polymer & Composites Science*, 2(2):47–56, 2016. doi: 10.1080/20550340.2016.1187434.

[76] K. Palanikumar. Experimental investigation and optimisation in drilling of GFRP composites. *Measurement*, 44(10):2138–2148, 2011. doi: 10.1016/j.measurement.2011.07.023.

[77] B. Latha and V.S. Senthilkumar. Modeling and analysis of surface roughness parameters in drilling GFRP composites using fuzzy logic. *Materials and Manufacturing Processes*, 25(8):817-827, 2010. doi: 10.1080/10426910903447261.

[78] F. Ficici. Evaluation of surface roughness in drilling particle-reinforced composites. *Advanced Composites Letters*, 29:1–11, 2020. doi: 10.1177/2633366X20937711.